Applied Catalysis B: Environmental 342 (2024) 123427

Contents lists available at ScienceDirect

Applied Catalysis B: Environmental

journal homepage: www.elsevier.com/locate/apcatb

A general strategy to enhance hydrogen peroxide generation via two-electron water oxidation by antimony modification for removal of triethyl phosphate and hexavalent chromium

Quan Zhou [a,1], Zaoxue Yan [b,1], Yangchun Lan [c,1], Zheshun Ou [a], Ruiting Hu [a], Xiaoli Wang [a], Zexi Yang [d], Yilin Chen [d], JunJie Cai [e], Qihong Lu [a], Shanquan Wang [a], Jimmy C. Yu [f], Lejing Li [g], Zhuofeng Hu [a,*]

[a] School of Environmental Science and Engineering, Guangdong Provincial Key Laboratory of Environmental Pollution Control and Remediation Technology, Sun Yat-sen University, Guangzhou 510006, China
[b] School of Chemistry and Chemical Engineering, Jiangsu University, Zhenjiang 212013, PR China
[c] School of Microelectronics, Southern University of Science and Technology, Shenzhen 518055, PR China
[d] School of Pharmaceutical Sciences, Sun Yat-sen University, Guangzhou 510006, China
[e] School of Materials and Energy, Guangdong University of Technology, Guangzhou 510006, China
[f] Department of Chemistry, The Chinese University of Hong Kong, New Territories, Shatin, Hong Kong, China
[g] Analytical Chemistry - Center for Electrochemical Sciences (CES), Faculty of Chemistry and Biochemistry, Ruhr University Bochum, Universitätsstr. 150, D-44780 Bochum, Germany

ARTICLE INFO

Keywords:
$CuWO_4$
Electrocatalysis
Hydrogen peroxide
Water oxidation
Hexavalent chromium (VI) reduction

ABSTRACT

Two-electron water oxidation has attracted more and more attention for H_2O_2 production. This strategy mainly uses water and does not require bubbling of oxygen gas, which can be widely used in oxygen-deficient environments. Currently, the most important research for two-electron water oxidation is the design of high-efficiency anode materials. Herein, a general method is developed to enhance the activity of two-electron water oxidation for H_2O_2 production via Sb_2O_3 modification. This strategy is suitable for a series of electrodes, including carbon fiber paper, graphite plate, WO_3, $CuWO_4$ and WO_3&$CuWO_4$ composite. The mechanism for Sb_2O_3 modification toward enhanced H_2O_2 generation is clearly demonstrated. It should be due to three factors: 1) enhance the reaction kinetic, 2) enlarge the specific surface area and 3) suppress H_2O_2 decomposition. According to density function calculation, it is firstly found that the Sb optimizes the Gibbs free energy of adsorbed *OH intermediate of its nearby atom, making its adjacent atom (such as W) the active site. Finally, these Sb-modified electrodes are firstly used to produce H_2O_2 for high-efficiency removal of triethyl phosphate, an environmental pollutant that are difficult to be degraded. It can also be used for the removal of hexavalent chromium, one kind of heavy metal.

1. Introduction

H_2O_2 is an important chemical in environmental treatment. For example, it can be oxidant for advanced oxidation process to removal organic pollutant. It can also be reducing agent for hexavalent chromium reduction. The application of H_2O_2 is convenient because it is in the form of liquid, which will not produce any byproduct of solid precipitate (such as iron sludge). Importantly, it is environmental-friendly because it only contains element of hydrogen and oxygen.

The current mainstream hydrogen peroxide production method is Anthraquinone oxidation (AO) method. However, this method requires high energy consumption, large-scale facilities, hydrogen source and noble metal catalysts like Pd [1]. At the same time, the storage and transportation of large amounts of concentrated H_2O_2 also poses safety hazards. The generated H_2O_2 suffer from serious decomposition during storage, thereby leading to low utilization efficiency. In order to avoid the disadvantages of the traditional H_2O_2 preparation process, there is a push to develop a more energy-efficient and resource-efficient route that

* Corresponding author.
E-mail address: huzhf8@mail.sysu.edu.cn (Z. Hu).
[1] Quan Zhou, Zaoxue Yan and Yangchun Lan contributes equally to this work

https://doi.org/10.1016/j.apcatb.2023.123427
Received 14 August 2023; Received in revised form 27 September 2023; Accepted 21 October 2023
Available online 24 October 2023

is amenable to on-site production of H_2O_2 in dilute working concentrations. Electrocatalytic synthesis of H_2O_2 is a green promising approach. The H_2O_2 can accumulate in useful concentrations over continued electrolysis. Currently, the two-electron oxygen reduction reaction (ORR, Eq. 1) is the mainstream method for the electrochemical generation of H_2O_2 [2].

$$O_2 + 2\,H^+ + 2e^- \rightarrow H_2O_2\ E^\circ = +0{\cdot}70\ \text{V vs·RHE} \quad (1)$$

However, the introduction of high purity oxygen gas is necessary during the two-electron ORR method to induce oxygen in the solution. The bubbling process is energy consuming and the use of high-purity oxygen is inconvenient and not safe. Also, this method is greatly limited by the solubility of oxygen (8 mg/L at 25 °C, 1 atm) and low diffusion coefficient of oxygen (2.1×10^{-5} cm^{-2} s^{-1}) in water. Finally, it is very inconvenient to use this method if oxygen is not accessible.

Recently, another H_2O_2 production method on the base of electrochemical two-electron water oxidation is developed (Eq. 2) [3–6].

$$2\,H_2O \rightarrow H_2O_2 + 2(H^+ + e^-)\ E^\circ = +1{\cdot}76\ \text{V vs·RHE} \quad (2)$$

The two-electron water oxidation process only requires inexpensive water to be the reactant. Because it does not require oxygen, this method is suitable to anaerobic environment such as sewer and black-odorous water. Therefore, the electrochemical two-electron water oxidation method to produce H_2O_2 is a promising low-cost strategy for H_2O_2 generation. To data, to obtain H_2O_2 effectively, design of high-efficiency anode material is crucial.

Currently, $BiWO_4$ [6], ZnO [7], $CaSnO_3$ [8], boron-doped diamond (BDD) [9] has been reported to be used as anode material in two-electron water oxidation. Recently, oxysalt is found to be one kind of high-efficiency for two-electrons water oxidation to H_2O_2. [10,11] For example, $LaAlO_3$ reaches an overpotential of 510 mV at 10 mA cm-2, lower than those of many reported metal oxide catalysts. Besides, $LaAlO_3$ maintains a stable Faradaic efficiency of H_2O_2 generation with only a 3% decrease after 3 h at 2.7 V vs. RHE. [12] Similar, $ZnGa_2O_4$ also with dual active sites exhibit very low overpotential and high selectivity for two electro water oxidation. The Faradaic efficiency reaches 82% at 2.3 V versus RHE for H_2O_2 generation. [3] Current, $CuWO_4$ has attracted more and more attention. According to the previous study [13], the binding energy of OH* on WO_3 (1.66 eV) makes it a suitable catalyst for the selective 2e-water oxidation reaction. At the same time, the range for six W-O distance in $CuWO_4$ is almost the same as that in monoclinic WO_3, [14–16] which can ensure the similar crystal field (a distorted and tilted WO_6 octahedron) of off-centered W in both compound. Besides, hybridization of Cu(3d)-O(2p) improves the chemical stability due to the strong covalency in metal-oxo bonds. [17,18] Numerous efforts have revealed that the oxygen chemisorption strength on a metal surface is related to its electronic structure, i.e. the position of the metal's d-band center relative to its Fermi level. [19–22] In our design, those transition metal (TM) atoms such as Co, Ni, Fe, Mn et. al featuring suitable chemisorption of oxygen on the catalyst surface were excluded because *OH can be easily dissociated into *O and finish the 4e-oxidation pathway. By contrast, W is found to be beneficial to generate H_2O_2.

Recently, the antimony (Sb) has attracted more and more attention in H_2O_2 generation. With the electron structure of $4d^{10}5\,s^25p^3$, Sb is one of the main group elements. Recently, it is reported that Sb single atom loaded C_3N_4 exhibits an apparent quantum efficiency of 17.6% at 420 nm and a solar-to-chemical conversion efficiency of 0.61%. [23] The Sb element play a key role in the photocatalytic two-electron oxygen reduction. [24] Sb atomic sites is end-on type, which promotes formation of Sb-μ-peroxide (Sb-OOH), leading to an efficient 2e- ORR. This means that the Sb will greatly influence the important intermediate during the formation of H_2O_2. In two-electron water oxidation, pure Sb_2O_3 has been reported to be able to produce H_2O_2. [25] However, previous report did not clear demonstrate the function of Sb and the mechanism for Sb during the two-electron water oxidation is still unknown. In our opinion, Sb should be an important species that can used for high-efficiency two-electron water oxidation for H_2O_2 production and application.

Herein, we firstly discover that Sb_2O_3 modification can be a general method to enhance the activity of two-electron water oxidation for H_2O_2 production on a series of electrodes, including carbon fibre paper, graphite plate, WO_3, $CuWO_4$ and WO_3&$CuWO_4$ composite. Importantly, the mechanism for Sb_2O_3 modification toward enhancing H_2O_2 generation is clearly demonstrated. It should be due to three factors: 1) enhance the reaction kinetically, 2) enlarge the specific surface area and 3) suppress H_2O_2 decomposition. According to density function calculation, it is firstly found that the Sb optimize the Gibbs free energy of adsorbed *OH intermediate of its nearby atom, making its adjacent atom (such as W) as the active site. Finally, these Sb modified electrode is firstly used to produce H_2O_2 for high-efficiency removal of triethyl phosphate, an environmental pollutant that are difficulty to degraded. It can also be used for the removeal of hexavalent chromium, one kind of heavy metals.

2. Experimental section

2.1. Reagents

Sources of reagents are provided in the Supporting Information (SI) Text S1.

2.2. Preparation of hydrophobic porous carbon fibre paper anode (CFP-PTFE)

the hydrophobic porous carbon fibre paper anode (CFP-PTFE) was converted from porous carbon fibre paper (CFP). Firstly, 2 * 4 cm^2 230-μm-thick CFP was soaked into 5%, 20% or 60% PTFE aqueous solution for 10 mins and then dried at 120 °C in a drying oven. 5% and 20% PTFE solutions were diluted from 60% PTFE. Then, the PTFE-treated CFP were annealed at 350 °C under nitrogen atmosphere for 30 mins to obtain a super-aerophilic surface. [30] The calcination is to enhance the interaction between catalyst and the substrate, therefore increasing the current density. The sample is called CFP-5%, CFP-20% and CFP-60%, respectively.

2.3. Preparation of hydrophobic CFP-CuBC electrode

Firstly, CuBC is prepared. 0.2 g of $CuSO_4$ and 2.0 g of glucose is dissolved in 20 ml of pure water and transfer to a 20 ml autoclave. Then, it was heat at 180 °C for 7 h and the precipitate was obtained by centrifugation. Subsequently, the precipitate is heat under 2 atmosphere at 1000 °C with the elevating rate of 5 °C per min, hold at 1000 °C for 3 h and cool to room temperature with the decreasing rate of 5 °C per min. They product is CuBC. Then the CuBC is dispersed in 0.05 wt% Nafion solution and drop-coated on the CFP-20% with the area of 2 cm^2. After being dried, the CFP-CuBC electrode is obtained.

2.4. Preparation of $CuWO_4$&WO_3-loaded porous carbon fibre paper anode (CFP-$CuWO_4$&WO_3)

To prepare $CuWO_4$ powder, firstly $Cu(NO_3)_2$ and ammonium meta tungstate hydrate was dissolved in dimethoxyethane in a molar amount of 2:1 to form the precursor of Cu and W with a concentration of 0.05 M. Then 0.4 ml nitric acid and 40 mg ammonium nitrate were added into 5 ml of above solution under constant stirring, followed by mixed with 100 mg commercial carbon black and stirred for 12 h at room temperature. Powder mixture of $CuWO_4$ and WO_3 catalyst was obtained after drying at 120 °C for 2 h and heating at 580 °C for 3 h in air.

To prepare a $CuWO_4$&WO_3-loaded porous carbon fibre paper anode (CFP-$CuWO_4$&WO_3), 10 mg mixture of $CuWO_4$ and WO_3 ($CuWO_4$&WO_3) was loaded on a slice of 2 * 4 cm^2 230-μm-thick CFP-

PTFE by the adhesive of 0.1 ml of 60% PTFE solution. Firstly, 10 mg nanoscale $CuWO_4$&WO_3 powder was dispersed onto 0.1 ml of 60% PTFE solution ultrasonically treated for 10 mins to disperse $CuWO_4$ powder evenly in the solution. Then, the $CuWO_4$&WO_3 powder suspension was drop-coated onto the 2 * 2 cm^2 part of CFP-PTFE and dry at 120 °C for 30 mins. At last, the $CuWO_4$&WO_3-treated CFP-PTFE were annealed at 350 °C under nitrogen atmosphere for 30 mins to get the CFP-$CuWO_4$&WO_3 anode.

2.5. Preparation of WO_3-loaded porous carbon fibre paper anode (CFP-WO_3)

To prepare WO_3 powder, firstly ammonium meta tungstate hydrate was dissolved in dimethoxyethaneto form the precursor of W with a concentration of 0.05 M. Then 0.4 ml nitric acid and 40 mg ammonium nitrate were added into 5 ml of above solution under constant stirring, followed by mixed with 100 mg commercial carbon black (Ketjen Black, ECP 600, Japan) and stirred for 12 h at room temperature. Powder WO_3 catalyst was obtained after drying at 120 °C for 2 h and heating at 580 °C for 3 h in air.

To prepare a WO_3-loaded porous carbon fibre paper anode (CFP-WO_3), 10 mg WO_3 was loaded on a slice of 2 * 4 cm^2 230-μm-thick CFP-PTFE by the adhesive of 0.1 ml of 60% PTFE solution. Firstly, 10 mg nanoscale WO_3 powder was dispersed onto 0.1 ml of 60% PTFE solution ultrasonically treated for 10 mins to disperse WO_3 powder evenly in the solution. Then, the $CuWO_4$ powder suspension was drop-coated onto the 2 * 2 cm^2 part of CFP-PTFE and dry at 120 °C for 30 mins. At last, the WO_3-treated CFP-PTFE were annealed at 350 °C under nitrogen atmosphere for 30 mins to get the CFP-WO_3 anode.

2.6. Preparation of $CuWO_4$-loaded porous carbon fibre paper anode (CFP- $CuWO_4$)

To prepare $CuWO_4$ powder, firstly powder of Cu_2O and WO_3 are thoroughly mixed and ground in a molar amount of 1:1, then heat at 850 °C for 3 h in air. To prepare a $CuWO_4$-loaded porous carbon fibre paper anode (CFP-$CuWO_4$), 10 mg $CuWO_4$ was loaded on a slice of 2 * 4 cm^2 230-μm-thick CFP-PTFE by the adhesive of 0.1 ml of 60% PTFE solution. Firstly, 10 mg nanoscale $CuWO_4$ powder was dispersed onto 0.1 ml of 60% PTFE solution ultrasonically treated for 10 mins to disperse $CuWO_4$ powder evenly in the solution. Then, the $CuWO_4$ powder suspension was drop-coated onto the 2 * 2 cm^2 part of CFP-PTFE and dry at 120 °C for 30 mins. At last, the $CuWO_4$-treated CFP-PTFE were annealed at 350 °C under nitrogen atmosphere for 30 mins to get the CFP-$CuWO_4$ anode.

2.7. Preparation of Sb_2O_3 modified electrodes

10 mg of sample powders (such as CuBC, $CuWO_4$, WO_3, $CuWO_4$&WO_3) and 10 mg of F_6NaSb was mixed by 0.1 ml of 60% PTFE solution and ultrasonically treated for 10 mins to disperse the powder evenly in the solution. Then, the suspension was drop-coated onto the 2 * 2 cm^2 part of CFP-PTFE and dry at 120 °C for 30 mins. At last, it was annealed at 350 °C under nitrogen atmosphere for 30 mins to get the Sb_2O_3 modified electrode. The sample are called as CFP-CuBC-Sb, CFP-$CuWO_4$&WO_3-Sb, CFP-$CuWO_4$-Sb and CFP- WO_3-Sb.

2.8. Preparation of CPF-Sb and C-Sb electrodes

10 mg of F_6NaSb was mixed by 0.1 ml of 60% PTFE solution and ultrasonically treated for 10 mins to disperse the powder evenly in the solution. Then, the suspension was drop-coated onto the 2 * 2 cm^2 part of CFP-PTFE and dry at 120 °C for 30 mins. At last, it was annealed at 350 °C under nitrogen atmosphere for 30 mins to obtain the CPF-Sb electrode. Similarly, when the suspension was drop-coated on a graphite plate, the obtained electrode is called C-Sb electrode.

2.9. Preparation of a series of Sb_2O_3 modified electrodes on CFP

10 mg of sample powders (such as CuBC, $CuWO_4$, WO_3, $CuWO_4$&WO_3) and 10 mg of F_6NaSb was mixed by 0.1 ml of 60% PTFE solution and ultrasonically treated for 10 mins to disperse the powder evenly in the solution. Then, the suspension was drop-coated onto the 2 * 2 cm^2 part of CFP-PTFE and dry at 120 °C for 30 mins. At last, it was annealed at 350 °C under nitrogen atmosphere for 30 mins to get the Sb_2O_3 modified electrode. The sample are called as CFP-CuBC-Sb, CFP-$CuWO_4$&WO_3-Sb, CFP-$CuWO_4$-Sb and CFP- WO_3-Sb.

2.10. Preparation of Fe-loaded porous carbon fibre paper cathode (CFP-NZVI)

To prepare a Fe-loaded CFP cathode, 10 mg nanoscale zerovalent iron (NZVI) was loaded on a slice of 2 * 4 cm^2 230-μm-thick CFP. Firstly, 10 mg nanoscale zerovalent iron (NZVI) was dispersed onto 0.1 ml of 0.05 wt% Nafion solution ultrasonically treated for 10 mins to disperse NZVI evenly in the solution. Then, the NZVI suspension was drop-coated onto the 2 * 2 cm^2 part of CFP and dry.

2.11. Electrocatalytic water oxidation test and analysis methods

The electrochemical tests were conducted with a CHI 760D electrochemical station controlled by a computer (CH Instruments, Inc., Shanghai) in a typical three-electrode system at room temperature. 2 M of $KHCO_3$ solution was used as the electrolyte in this work unless claimed, and the electrolyte was stirred at a rate of 60 rpm during the electrolysis.

The electrochemical tests were conducted in double-tank system. When the electrochemical test was set in double-tank system, there was a 2 * 2 cm^2 of proton exchange membrane set between two electrolytic tanks to prevent H_2O_2 produced on anode from moving to cathode tank, and the working electrode was set in the anode tank while the counter electrode and reference electrode were set in the cathode tank.

The H_2O_2 generation experiment was performed in double-tank system. A carbon rod electrode, Ag/AgCl electrode and the as-prepared anode were used as the counter, reference electrode and working electrode, respectively. 50 ml of electrolyte was used in each tank. After a short period of operation at different bias (1.66 V vs RHE to 3.66 V vs RHE), the generated concentration of H_2O_2 was quantified via N, N-diethyl-p-phenylenediamine (DPD)–horseradish peroxidase (POD) method.

The triethyl phosphate degradation test was performed. 10 ppm triethyl phosphate was added into the 50 ml of electrolyte before electrolysis. Then 1 ml of the solution was extracted by 0.2 ml ethyl acetate every 20 mins and the concentration of triethyl phosphate was determined by a Gas chromatography (Agilent GC7890).

The concentration of H_2 test was performed in a double-tank system with air tightness. 50 ml of electrolyte was used in each 150-ml-tank. 1 ml of air in cathode tank was drawn out by a syringe then injected into a Gas chromatography (Agilent GC7890) every 30 mins.

2.12. H_2O_2 measurement method

This H_2O_2 measurement method is based on the oxidation of DPD by H_2O_2 with the assistant of POD, oxidation product of DPD is a pink compound with strong absorption peaks at 510 and 551 nm. The absorption intensity of the mixture solution at 551 nm were recorded, then the concentration of H_2O_2 can be calculated through the prepared standard curves. In detail, 0.1 g DPD was dissolved in 10 ml 0.05 M H_2SO_4 as solution a. 10 mg POD was dissolved in 10 ml deionized water (DI) as solution b. 0.5 M phosphate solution with pH value of 5.6 was used as buffer. 1.7 ml buffer was added into 0.3 ml testing sample, then add a solution and b solution 0.05 ml respectively in sequence. Finally, after waiting for 40 s, the absorption of the mixture at 551 nm was

recorded with UV–vis spectrometer.

2.13. Hexavalent chromium (Cr(VI)) reduction test

The Hexavalent chromium (Cr(VI)) reduction test was performed in a double-tank system, 50 ml of electrolyte was used in each tank. After a short period of operation at different bias (1.66 V vs RHE to 3.66 V vs RHE), 1.5 ml of electrolyte in the anode electrolytic cell was taken out at intervals and mixed with 1.5 ml of different concentration of potassium dichromate solution for 10 mins. Then, the mixed solution was extracted and the residual concentration of Cr(VI) was quantified via Diphenyl semicarbazide method (Text S2 in SI) by UV–vis spectrometer with an excitation wavelength of 548 nm. In detail, 5 mg of diphenyl semicarbazide was dissolved in 10 ml 1.8 M H_2SO_4 as solution c. 0.3 ml of solution c was added into 3 ml of testing sample. Finally, after waiting for 10 mins, the absorption of the mixture at 548 nm was recorded with UV–vis spectrometer.

2.14. Theoretical calculations

The Vienna Ab initio simulation package (VASP) was used for all the calculations in this article. [26,27] We applied projector-augmented-wave method with Perdew–Burke–Ernzerhof GGA functional. [28,29] Electronic convergence limit was set to be 1×10^{-4} eV. Optimization of atomic coordinates was considered to be converged if Hellmann–Feynman force was smaller than 2×10^{-2} eV $Å^{-1}$. The size of unit cell is a= 11.6 Å, b= 9.74 Å, c= 18.72 Å, the facet is (001) and it contain 7 W, 8 Cu, 33 O, 1 Sb and 1 H. The vacuum region is about 15 Å in height.

3. Results and discussion

3.1. H_2O_2 production on PTFE-CFP electrode

PTFE of different concentration was loaded on pristine CFP to prepared CFP-PTFE anode. The 4 different anodes (pristine CFP, CFP-5%, CFP-20%, CFP-60%) were used to generate H_2O_2 by oxidating water in the anode cell with the bias of 3.16 V vs. RHE (Text S4 in SI)·H_2O_2 is measure by PDP method (Experiment section and Fig. S1) CFP-20% performed the best in this system for oxidating water to H_2O_2 as a substrate anode material (Figs. S2–3). Therefore, it is used as the substrate to prepare other electrodes. The preparation step is shown in experimental section and shown schematically in Fig. S4.

3.2. H_2O_2 production on $CuWO_4$, WO_3 and $CuWO_4$&WO_3 electrodes

In the double-tank system, we used CFP-20% as the base anode to prepare CFP-$CuWO_4$, CFP-WO_3 and CFP-$CuWO_4$&WO_3. The crystallographic pattern of the as-prepared $CuWO_4$, WO_3 and $CuWO_4$&WO_3 are shown in Fig. 1a-c. The peaks found were compared to the ICSD database. The peak at 18.2°correspond to the PTFE. The SEM image of $CuWO_4$, WO_3 is shown in Fig. S5.

The H_2O_2 generation performance of CFP-$CuWO_4$ anode, CFP-WO_3 anode and CFP-$CuWO_4$&WO_3 anode at the bias of 3.16 V vs RHE was also investigated as shown in Fig. 1d, indicating that the CFP-$CuWO_4$&WO_3 anode made of $CuWO_4$ and WO_3 mixture is superior to pure $CuWO_4$ or WO_3 for producing H_2O_2 at the bias of 3.16 V vs RHE. Similar trend can be found at higher potential of 3.66 V vs. RHE (Fig. S6). This proves that the yield of hydrogen peroxide reaches the highest (1.29 mmol/L) under the condition of 3.16 V vs RHE.

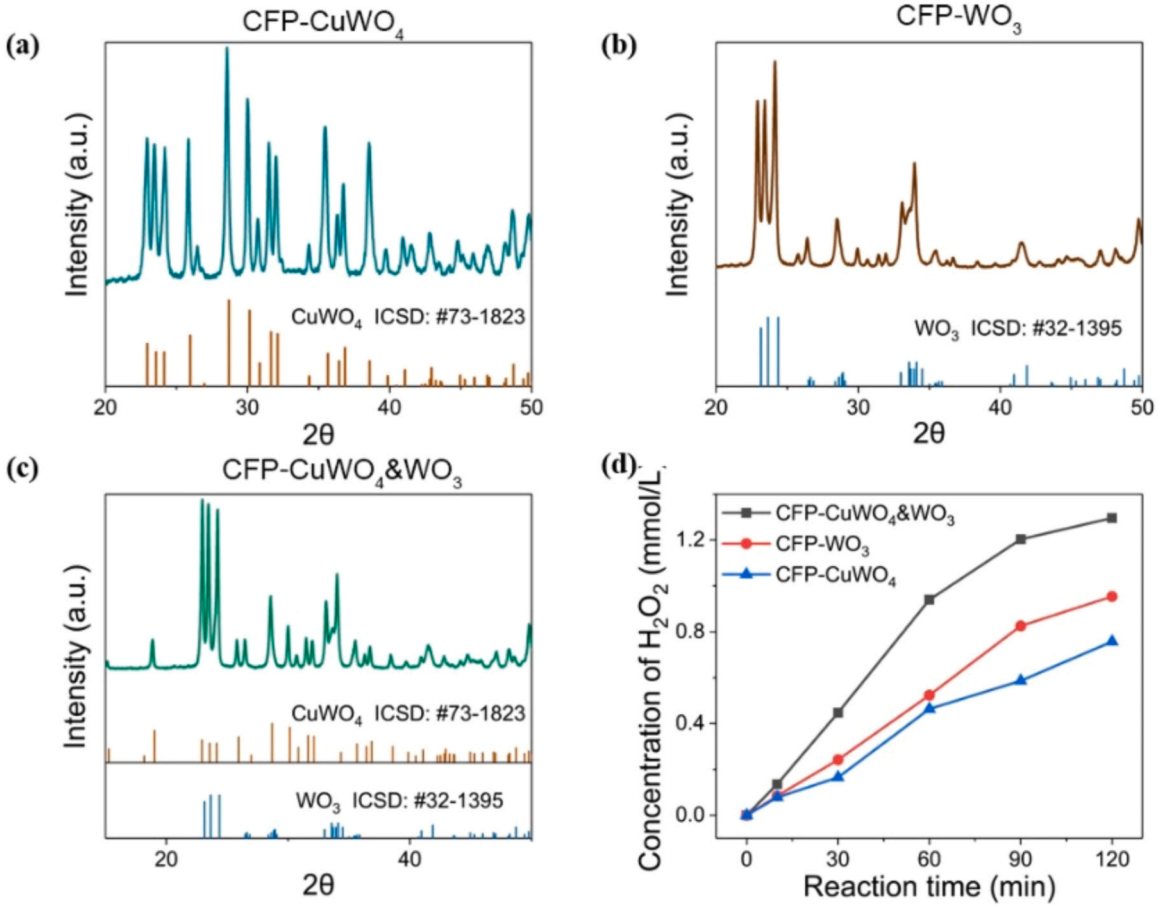

Fig. 1. XRD patterns of (a) $CuWO_4$, (b) WO_3. (c) $CuWO_4$&WO_3 powder. (d) Time profiles of the H_2O_2 generation at the bias of 3.16 V vs RHE of different anodes.

Fig. 2a shows the morphology of $CuWO_4$&WO_3 samples. It is spherical shape of $CuWO_4$ with the nanoparticle size of 250 nm. X-ray photoelectron spectroscopy analysis was carried out to further characterize the chemical surface state of the $CuWO_4$&WO_3. Fig. 2b presents the XPS survey spectra. Peak related to Cu, W, O, and C can be found, which are in agreement with the single-phase samples observed in the XRD results. Fig. 2c presents the W 4 f high-resolution spectra of the $CuWO_4$&WO_3 powder, where three peaks related to W 4 f 7/2 (35.3 eV), W 4 f 5/2 (37.5 eV) and W 5p 3/2 (41.2 eV) could be noted [31], which related to the W^{6+}. The core level of Cu 2p is shown in Fig. 2d. The peaks found in the vicinity of 934.3 eV and 954.1 eV are attributed to Cu 2p 3/2 and Cu 2p ½, while the peaks show up near 945 eV are satellite peaks commonly observed in Cu^{2+} compounds [32].

3.3. Effects of Sb_2O_3 modification on H_2O_2 production

In order to further increase the yield of H_2O_2, we try to modify the CFP-$CuWO_4$&WO_3.electrodes with Sb_2O_3. Fig. 3a shows the XRD pattern of CFP-$CuWO_4$&WO_3-Sb, which indicate the presence of Sb_2O_3. EDS and mapping of CFP- $CuWO_4$&WO_3-Sb surface (Figs. S7–9) shows that Sb has been introduced. To investigate interaction between the Sb and the substrate, X-ray photoelectron spectroscopy (XPS) measurements were conducted (Fig. S10). The binding energy of Sb 3d for CFP-$CuWO_4$&WO_3-Sb ($Sb_3d_{3/2}$ at 540.0 eV and $Sb_3d_{5/2}$ at 530.5 eV) is close to the oxidation state of Sb^{3+} ($Sb_3d_{3/2}$ at 539.8 eV and $Sb_3d_{5/2}$ at 530.5 eV). [30].

The H_2O_2 generation rate is compared on CFP-$CuWO_4$&WO_3 and CFP-$CuWO_4$&WO_3-Sb at different potentials (Fig. 3b-d). Below 2.16 vs. RHE, no H_2O_2 can be generated no matter Sb_2O_3 is introduced or not. They both reach the climax at 3.16 V vs. RHE. The CFP-$CuWO_4$&WO_3-Sb electrode exhibits a rate of 1.25 mmol/L/h, which is much higher than that of 0.62 mmol/L/h on the Sb-free sample, strongly demonstrate the enhancement induced by the Sb_2O_3. After 3.66 V, the generation rate of H_2O_2 decrease because the four-electron water oxidation to O_2 become more apparent. Interestingly, it is found that the accumulation of H_2O_2 become slower and slower at the Sb-free sample, while is maintain or even accelerate at the Sb_2O_3 sample, indicating the Sb_2O_3 also beneficial to the accumulation of the H_2O_2.

This method is a general method that can also be used for different electrodes. Besides CFP-$CuWO_4$&WO_3-Sb, it is found that the modification can used to enhance two-electron water oxidation on other electrodes. The XRD pattern of them is shown in Fig. S11. The peak at 28.4° corresponds to the Sb_2O_3.which indicates that Sb_2O_3 has been introduced. For example, the Sb_2O_3 modified CFP (CFP-Sb, Fig. 4a, b), Sb_2O_3 modified graphite (C-Sb, Fig. 4c, d), Sb_2O_3 modified CFP-CuBC (CFP-CuBC-Sb, Fig. 4e, f), Sb_2O_3 modified CFP-$CuWO_4$ (CFP-$CuWO_4$-Sb, Fig. 4g, h), Sb_2O_3 modified CFP-WO_3 (CFP-$CuWO_3$-Sb, Fig. 4i, j) all shown higher activity than their Sb-free counterpart. This strongly indicates that the Sb_2O_3 modification strategy is a widely-accepted method to enhance the two-electron water oxidation for H_2O_2 generation.

3.4. Mechanism for the enhancement caused by the Sb_2O_3 modification

3.4.1. Promotion of the reaction kinetics

Firstly, the addition of Sb increases the reaction kinetics. Fig. S12 shows that Sb_2O_3 modified anode started to produce H_2O_2 at a lower bias than their Sb-free counterparts. This indicates that the introduction of Sb is beneficial to the water oxidation toward hydrogen peroxide generation. Furthermore, to investigate the process of hydrogen

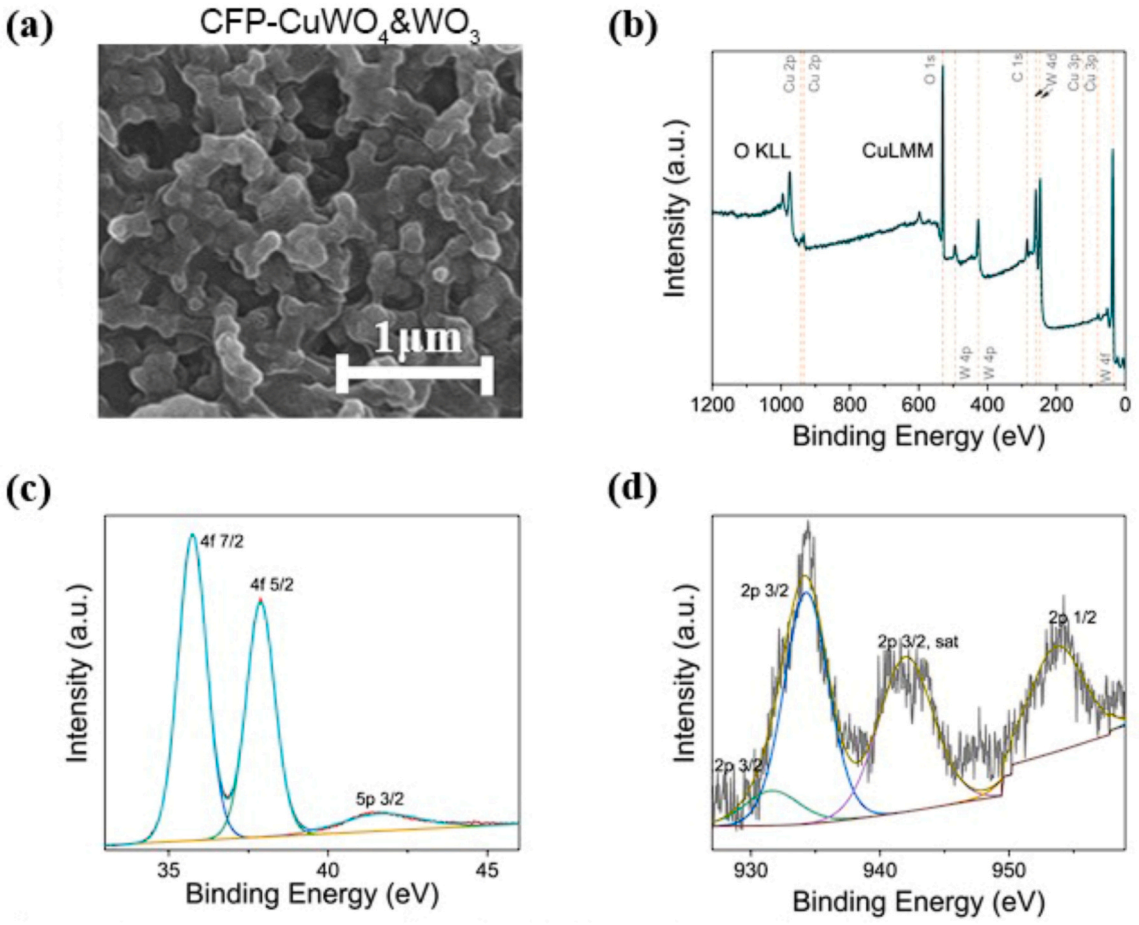

Fig. 2. (a) XRD pattern of $CuWO_4$&WO_3, (b)XPS survey spectra of $CuWO_4$&WO_3. XPS spectrum of (c) W 4 f and (d) Cu 2p.

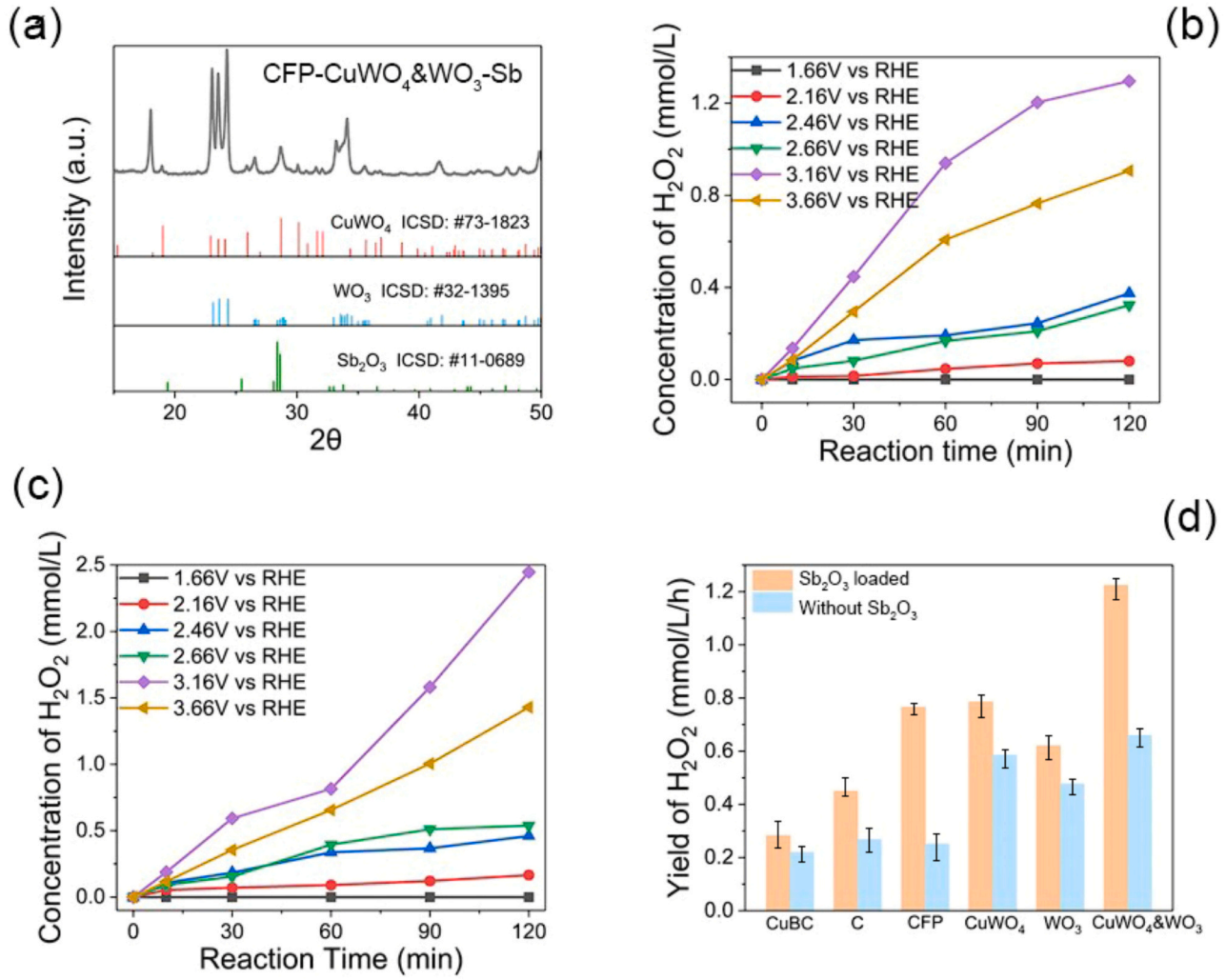

Fig. 3. (a) XRD pattern of CFP-$CuWO_4$&WO_3-Sb. The three bottom patterns are the Inorganic Crystal Structure Databa of WO_3, $CuWO_4$ and Sb_2O_3. Time profiles of the H_2O_2 generation at different bias of (b) CFP-$CuWO_4$&WO_3 anode and (c) CFP-$CuWO_4$&WO_3-Sb anode. (d) Yield of the H_2O_2 generation at the bias of 3.16 V vs RHE using different anodes.

peroxide generation, density functional calculation is performed (Fig. 5a, b). It known that the adsorption of *OH is an important parameter for the evolution of H_2O_2 generation. [6] The charge of Gibbs free energy for *OH adsorption (ΔG_{OH^*}) should be at an optimal range of 1.6–2.4 eV. Larger value leads to OH radical generation, while smaller value leads to O_2 evolution. Density functional calculation shows that our Sb doped $CuWO_4$ is about 2.25 eV, which is in the optimal range. The introduction of Sb only slightly shift the ΔG_{OH^*} from 2.03 eV to 2.25 eV.

After structure relaxation, the *OH can be adsorbed on the substrate. The oxygen atom from the *OH is linked with the W atom from the substrate. It is interesting that the *OH is not at the Sb site. This indicates that the W atoms near the Sb are still the active sites for the H_2O_2 generation. The function of Sb is to optimize Gibbs free energy of the nearby atoms, therefore promoting their activity.

The theoretical potential of H_2O_2 generation via water oxidation is 1.76 vs. RHE. In the absence of bias, the first step of *OH adsorption is 2.25 eV and the step of H_2O_2 generation is 3.52 eV. At the bias of 1.27 V, the reaction needs to overcome a large barrier 0.98 eV in the first step although the second step does not need to overcome any barrier. At 1.76 V, the barrier for the first step is only 0.49 eV and the energy even drop on the second step. At a related large bias of 3.16 V, the energy continues to drops and the formation of H_2O_2 is favorable at this potential.

3.4.2. *Increase of the active sites*

Second, another advantage of the Sb introduction is the increase of specific surface area and corresponding active sites. As shown in the capacitance test by using the following equation.

$$C = \frac{I \times \Delta t}{\Delta V} \tag{3}$$

Where C is the capacitance, I is the constant current ΔV is the change of potential and Δt is the duration.

In our experiment, I and ΔV is kept as constants. The longer of Δt corresponds to large capacitance and related larger specific electrochemical surface area.

As shown in Fig. 5c, the CFP-$CuWO_4$&WO_3-Sb owned much larger capacitance than CFP- $CuWO_4$&WO_3, meaning that CFP-$CuWO_4$&WO_3-Sb has a nearly 50 times larger electrochemical surface area than CFP-$CuWO_4$&WO_3 for producing H_2O_2. In the SEM image (Fig. S13), it can also be found that the morphology of the surface also changes after Sb modification. This increase of surface area helps to provide more active site and CFP-$CuWO_4$&WO_3-Sb performed better in this system for oxidating water to H_2O_2. Generally, the larger specific electrochemical surface area can also be observed in other electrodes including CPF, graphite (C), CFP-CuBC, $CuWO_4$ and WO_3 (Fig. S14), suggesting that the Sb modification is a general method to enhance the two-electron water oxidation by increasing the surface area.

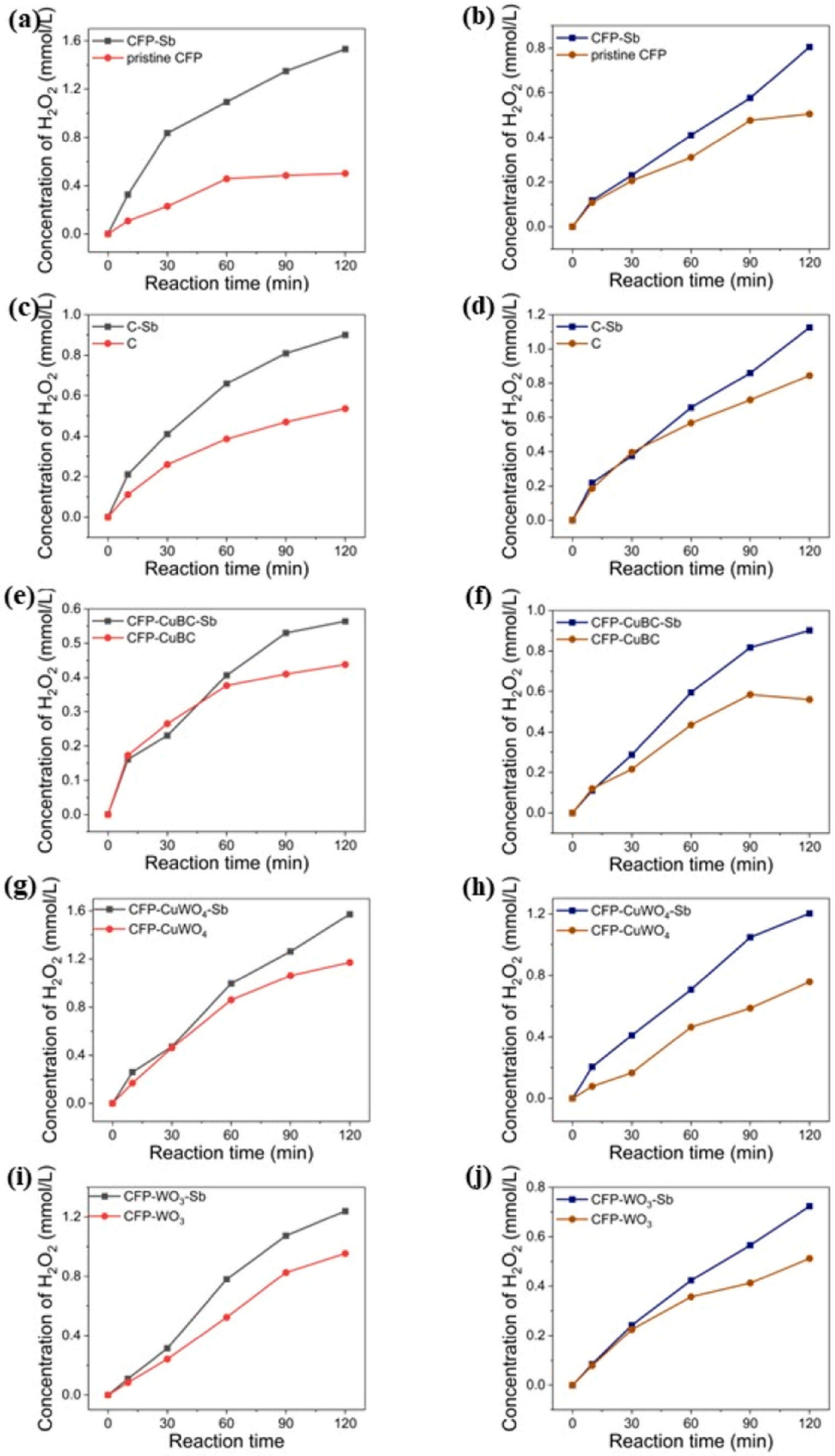

Fig. 4. Time profiles of the H_2O_2 generation of different anodes at the bias of (a)、(c)、(e)、(g)、(i) 3.16 V vs RHE and (b)、(d)、(f)、(h)、(j) 3.66 V vs RHE.

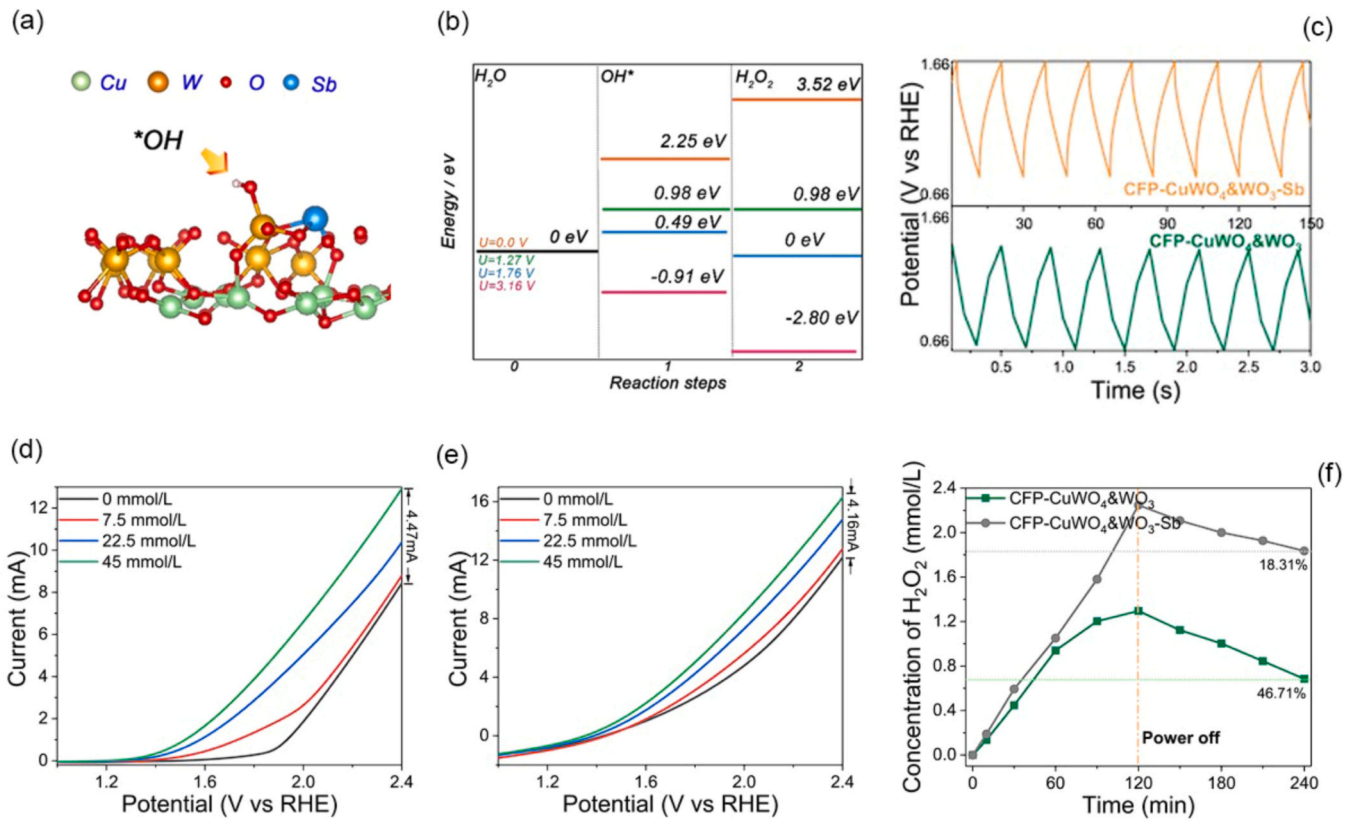

Fig. 5. (a) Structure of OH* on CFP-$CuWO_4$&WO_3-Sb, green spheres display the Cu atoms, red spheres display the O atoms, orange spheres display the W atoms, and blue spheres display the Sb atoms. (b) Energy diagram for H_2O_2 evolution on Sb-loaded CFP-$CuWO_4$&WO_3 (c) I-t curve of CFP-$CuWO_4$&WO_3 and CFP-$CuWO_4$&WO_3-Sb. The CVs of (d) CFP-$CuWO_4$&WO_3 and (e) CFP-$CuWO_4$&WO_3-Sb. (f)Time profiles of the H_2O_2 generation and decomposition of different anodes without or with H_2O_2 addition in anode cell (7.5, 22.5 and 45 mmol/L) in anode tank.

3.4.3. *Suppression of H_2O_2 decomposition*

Finally, the additional of Sb suppress the decomposition of generated H_2O_2 on the surface of the anode. In two-electron water oxidation, it is also possible that the generated H_2O_2 will be decomposed on the surface again, which adverse to the H_2O_2 generation. To study the decomposition of H_2O_2 on CFP-$CuWO_4$&WO_3 and CFP-$CuWO_4$&WO_3-Sb electrode, different concentrations of H_2O_2 were added to the anode electrolytic cell and recorded the current changes under different bias (Fig. 5d, e). When H_2O_2 is added, the current density will increase if H_2O_2 suffer from serious decomposition because it consumes electrons on the anode for anodic decomposition. The results shows that H_2O_2 is easier to decompose on CFP- $CuWO_4$&WO_3, the current density increase by about 4.47 $mAcm^{-2}$, while CFP-$CuWO_4$&WO_3-Sb anode shows the value of 4.16 $mAcm^{-2}$. Besides, we also monitor the concentration of H_2O_2 after the stop of electrolysis. At this stage, no new H_2O_2 are produced and the concentration of H_2O_2 will decrease. As shown in Fig. 5f, the decrease of H_2O_2 concentration is obviously slower on the Sb modified anode (18.31%) than that on the Sb-free sample (46.71%). Finally, we monitor a series of electrode and observe similar trend on the Sb modified electrode (Fig. 6, Table 1). Therefore, Sb is beneficial to suppress the H_2O_2 decomposition.

3.5. *Degradation of triethyl phosphate*

Organophosphorus acid esters (OPs) are a widely used substance group that are widely used in Flame retardants and plasticizers. As OPs cannot bonded chemically to the polymeric materials, they are easy to diffuse and be emitted into the environment, causing serious pollution. [31] OPs can migrate in different environmental media and have been detected in various environmental compartments. [31] Due to this they are insufficient degraded in sewage treatment plants and enter the aquatic environment. Therefore, their degradation and removal are of great significance. Currently, advanced oxidation process including photocatalysis and electrochemical oxidation method has been used for its degradation. [32–34].

Herein, we first attempt to use our two-electron water oxidation method for its degradation. Brief, CFP-$CuWO_4$&WO_3 and CFP-$CuWO_4$&WO_3-Sb is used as anode and a zero-valance iron electrode is used as cathode. In this system, the H_2O_2 generated from the anode could migrated to the cathode, and the nanoscale zerovalent iron are good catalysts to converse the H_2O_2 into OH radicals, therefore its activity in degradation of Triethyl phosphate.

The degradation of TEP on CFP-$CuWO_4$&WO_3-Sb at different bias is shown in Fig. 7a. It is obvious that the degradation rate is proportional to the generation rate of H_2O_2. The degradation first become faster and faster with increase potential as more H_2O_2 is generated. Then, it reaches the climax at 3.16 V vs. RHE. 10 ppm of TEM can be totally degraded. Then it begins to decrease when the potential is larger. At 3.16 V vs. RHE, it can be observed in the curve of the Gas chromatography that the peak related to TEP decrease (Fig. 7b). Within 6 h, the concentration of TEP decrease to almost zero (Fig. 7c, Fig. S15). Finally, the total organic carbon (TOC) also decreases with the degradation.

In addition, the effect of Sb modification is also investigated. CFP-$CuWO_4$&WO_3, CFP-$CuWO_4$ and CFP- WO_3 with and without Sb modification are used to degrade the TEP and result are shown in Fig. 8. Apparently, all the electrode with Sb exhibits better activity in the degradation of TEP, suggesting the promotion of the Sb. Their corresponding kinetic rate constant is shown in Fig. S16. In summary, Table 2 shows the generation rate of H_2O_2, TEP degradation rate and the kinetic rate constant.

Then, cycling experiment is performed. As shown in Fig. 9a, the degradation rate of the TEP maintain in three cycles. Almost all the TEP

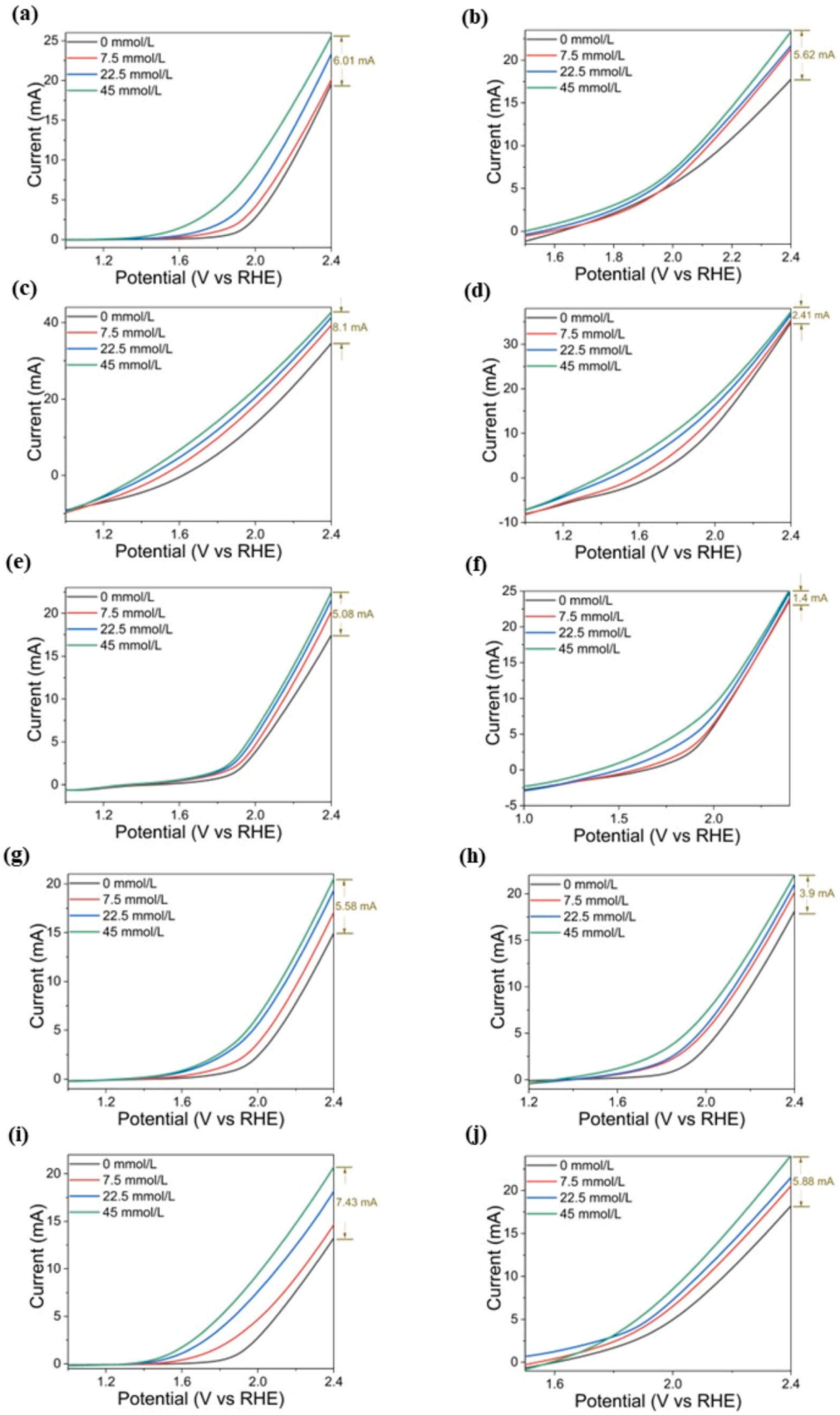

Fig. 6. the CVs of (a) CFP, (b) CFP-Sb, (c) C, (d) C-Sb, (e) CFP-CuBC, (f) CFP-CuBC-Sb, (g) CFP-$CuWO_4$, (h) CFP-$CuWO_4$-Sb, (i) CFP-WO_3 and (j) CFP-WO_3-Sb without or with H_2O_2 addition in anode cell (7.5, 22.5 and 45 mmol/L) in anode tank.

Table 1
Parameters of H_2O_2 decomposition in CV diagram of different anodes.

Anode	Increase of current at 2.4 V vs. RHE after adding 45 mM H_2O_2 (mA)	Current increase (%)
CFP-Sb	5.62	31.1
Pristine CFP	6.01	31.3
C-Sb	2.41	6.94
C	8.10	23.6
CFP-CuBC-Sb	1.40	5.94
CFP-CuBC	5.04	29.2
CFP-$CuWO_4$-Sb	3.90	21.6
CFP-$CuWO_4$	5.58	37.2
CFP-WO_3-Sb	5.58	32.3
CFP-WO_3	7.43	56.2
CFP-$CuWO_4$&WO_3-Sb	4.16	34.6
CFP-$CuWO_4$&WO_3	4.47	53.9

can be degraded, suggesting good stability of our system. The XRD of the CFP-$CuWO_4$&WO_3-Sb after cycling test is shown in Fig. 9b, which is also the same with that before used (Fig. 3a), meaning that its structure maintain. Besides, we also monitor the possible release of the Cu^{2+} and Sb^{3+} ions in the electrolyte. However, their concentration is very low. Therefore, this confirms our electrode has good stability.

3.6. Simultaneously hydrogen generation and CO_2 reduction at the cathode

The CFP-$CuWO_4$&WO_3-Sb an also be used as cathode simultaneously. As a cathode, the main reaction is water reduction to hydrogen and we observe a 14 $mmolL^{-1}h^{-1}$ hydrogen generation rate, which corresponds to a faradaic efficiency of about 95.5%. Interestingly, because $KHCO_3$ is the electrolyte, we firstly observe that CO_2 reduction occur at the cathode. 0.95 $mmolL^{-1}h^{-1}$ CO and 0.32 $mmolL^{-1}h^{-1}$ CH_4 are also found, which account for 3.7% and 0.8% Faradaic efficiency, respectively. This is the first time for the simultaneously H_2O_2 generation coupling with CO_2 reduction.

3.7. The reduction of Cr(VI)

The generated H_2O_2 can be used for the reduction of hexavalent chromium (potassium dichromate), a typical environmental pollutant. Briefly, 1.5 ml of the electrolyte in the anode cell was taken out at intervals and mixed with different concentrations of potassium dichromate solution to measure the reduction of hexavalent chromium. The reaction that should happen is listed below. In this reaction, H_2O_2 acts as a reducing agent, the reduction of Cr(VI) by H_2O_2 should be favored at

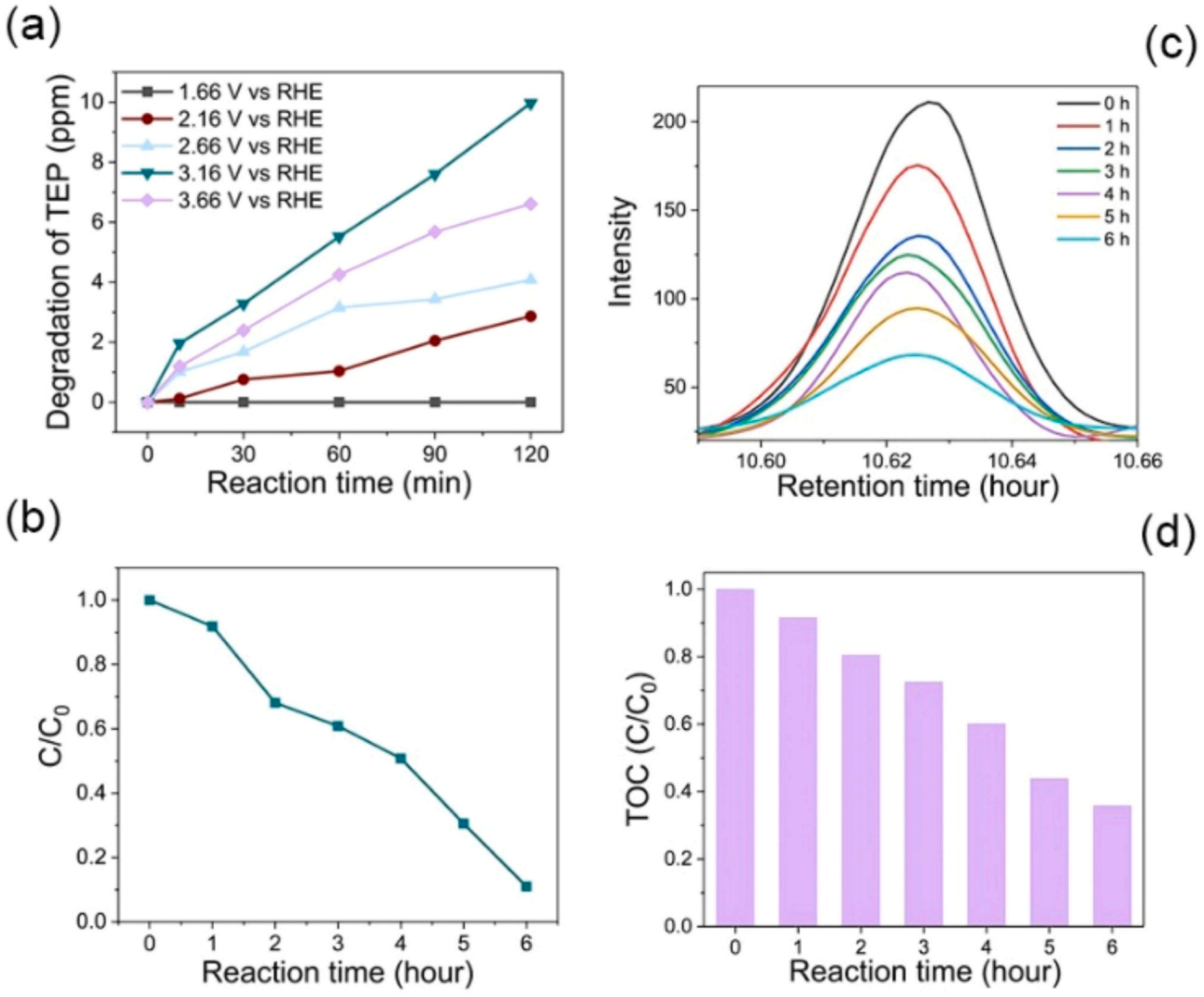

Fig. 7. (a) degradation of TEP at different potential. (b) time profile of HPLC showing the single of TEP. (c) Time profiles of the TEP removal (d) TOC degradation of TEP at the bias of 3.16 V vs RHE using CFP-$CuWO_4$&WO_3-Sb as anode and CFP-NZVI as cathode.

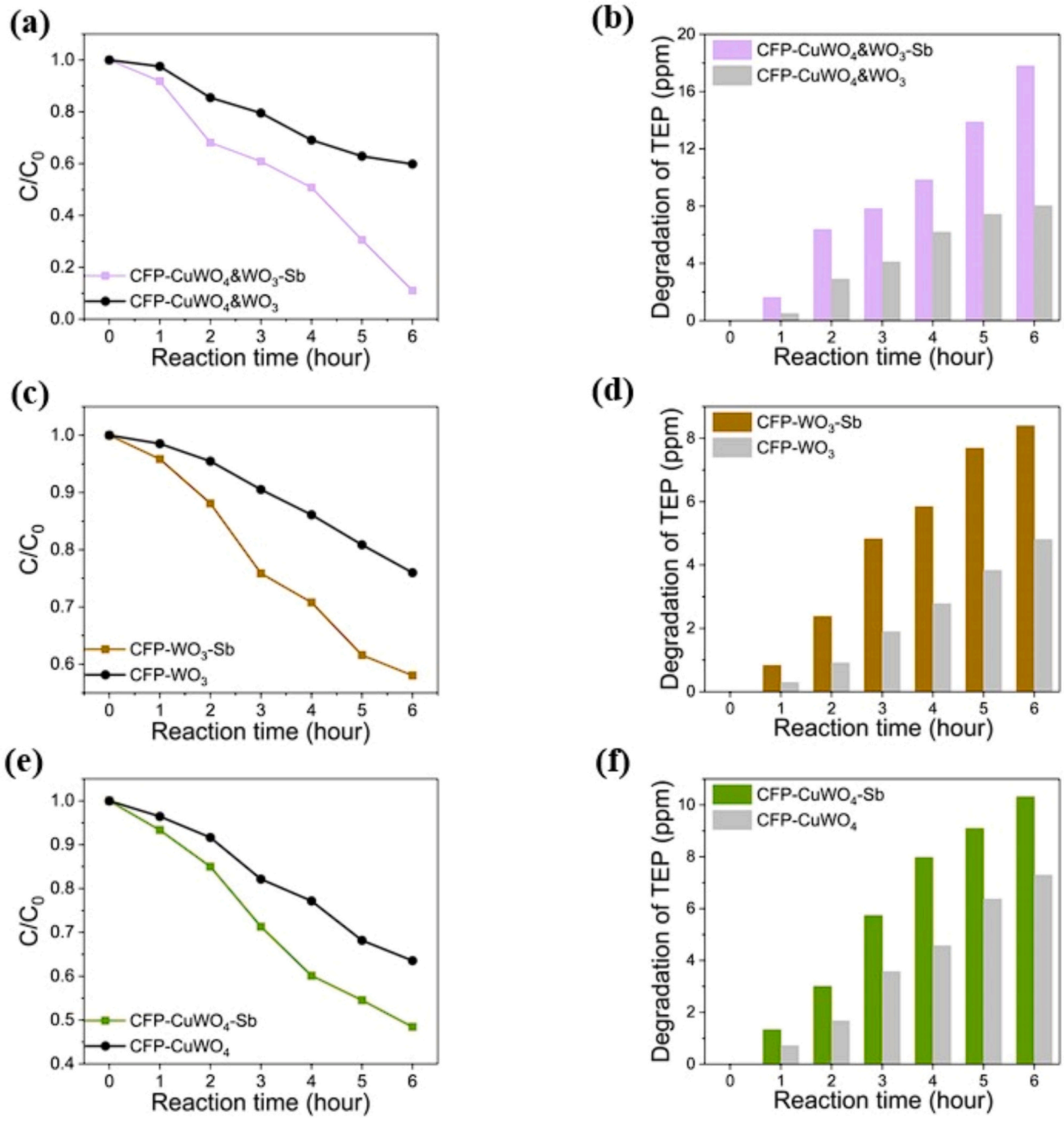

Fig. 8. Time profiles of the TEP removal in single-tank system at the bias of 3.16 V vs RHE using CFP-NZVI as cathode and (a), (b) CFP-$CuWO_4$&WO_3 with or without Sb_2O_3 loaded, (c), (d) CFP- WO_3 with or without Sb loaded, (e), (f) CFP-$CuWO_4$ with or without Sb_2O_3 loaded as anode.

Table 2
Yield of H_2O_2 and TEP degradation parameters of different anode.

Anode	Generation rate H_2O_2 (mmol/L/h	6 h TEP degradation rate (ppm)	Rate constant (k, $hour^{-1}$)
CFP-$CuWO_4$&WO_3-Sb	1.25	17.79	0.3252
CFP-$CuWO_4$&WO_3	0.62	8.03	0.0939
CFP-WO_3-Sb	0.61	8.39	0.0977
CFP-WO_3	0.43	4.80	0.0472
CFP-$CuWO_4$-Sb	0.80	10.31	0.1284
CFP-$CuWO_4$	0.59	7.29	0.0795

high concentrations of H_2O_2 and protons. [34].

$$2HCr^{6+}O_4^- + 3\ H_2O_2 + 8\ H^+ \rightarrow 2Cr^{3+} + 3\ O_2 + 8\ H_2O\ E_0 = 0{\cdot}65\ V_{NHE} \quad (4)$$

16.46 ppm of Cr(VI) could be reduced in 2 mins by using the generated H_2O_2 by H_2O_2 produced in the anode cell of system using CFP-$CuWO_4$&WO_3-Sb at the bias of 3.16 V vs RHE, while only 9.29 ppm of Cr (VI) was reduced by H_2O_2 produced by system using CFP-$CuWO_4$&WO_3 as anode (Fig. 4a-d). The result shows that with Sb modification on the CFP-$CuWO_4$&WO_3, the system using anode CFP-$CuWO_4$&WO_3-Sb could produce more H_2O_2 and reduce more Cr(VI) than the system using anode CFP-$CuWO_4$&WO_3. .

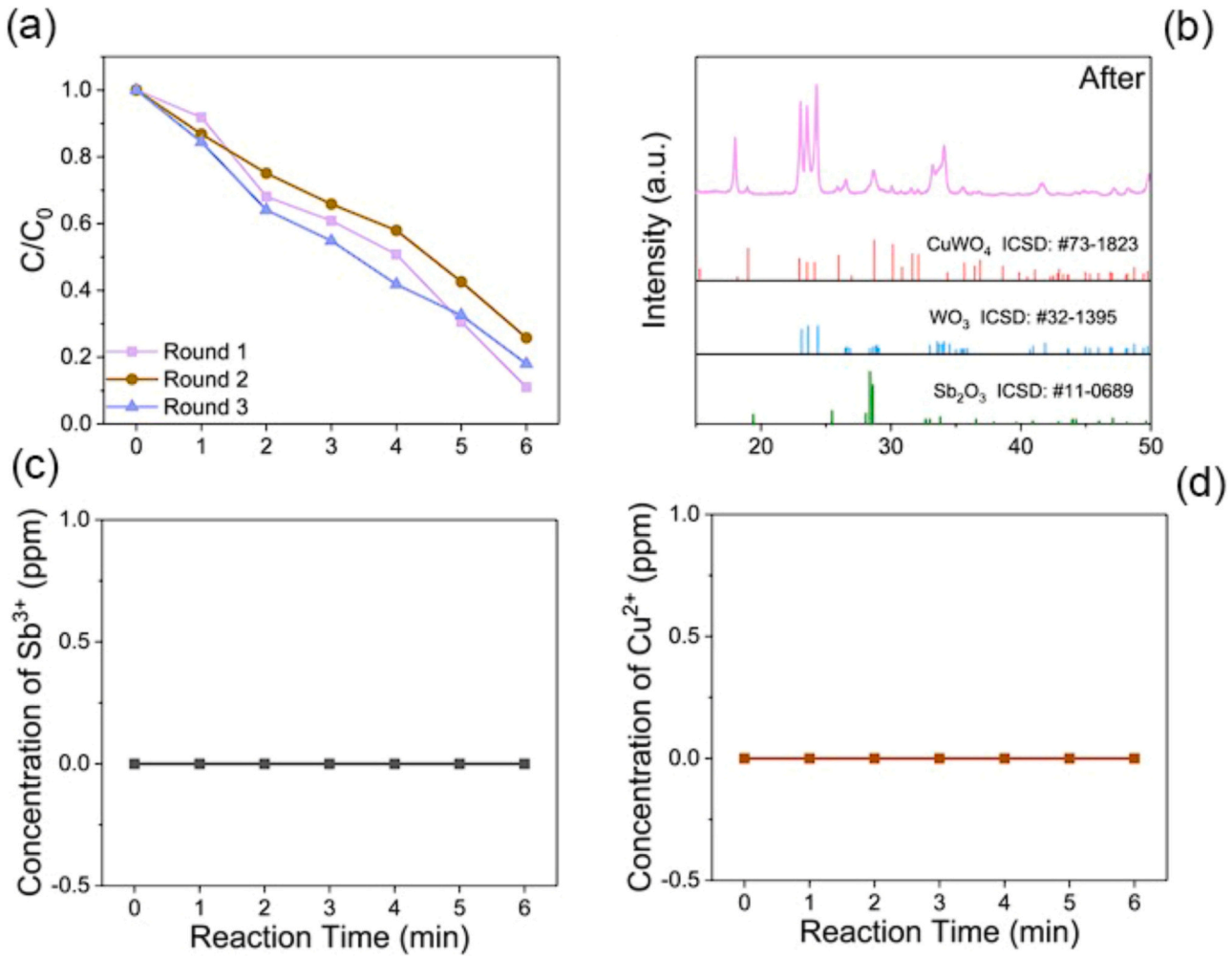

Fig. 9. (a) Time profiles of the TEP removal at the bias of 3.16 V vs RHE using CFP-$CuWO_4$&WO_3-Sb as anode and CFP-NZVI as cathode for three cycles. (b) XRD pattern of CFP-$CuWO_4$&WO_3-Sb after cyclic test. (c) Concentration of Cu^{2+} in the anodic cell electrolyte under the cycle test. (d) the concentration of Sb^{3+} in the anodic cell electrolyte under the cycle test.

4. Conclusion

In conclusion, we report a general strategy that can be used in a series of electrodes including carbon-based electrode and metal oxide electrodes. This strategy can promote water oxidation kinetic, increase specific surface area and avoid H_2O_2 decomposition. The two-electron water oxidation strategy is first used to remove triethyl phosphate and hexavalent chromium. The Sb is in the form of Sb_2O_3. The Sb modification is to accelerate the reaction kinetic, to increase the specific surface are of electrode and to suppress the decomposition of H_2O_2. The CFP-$CuWO_4$&WO_3-Sb electrode exhibits a rate of 1.25 mmol/L/h, which is much higher than that of 0.62 mmol/L/h on the Sb-free sample, strongly demonstrate the enhancement induced by the Sb_2O_3. The Sb modification strategy can be widely used in a series of electrode, including Sb_2O_3 modified CFP (CFP-Sb), Sb_2O_3 modified graphite (C-Sb), Sb_2O_3 modified CFP-CuBC (CFP-CuBC-Sb), Sb_2O_3 modified CFP-$CuWO_4$ (CFP-$CuWO_4$-Sb), Sb_2O_3 modified CFP-WO_3 (CFP-$CuWO_3$-Sb), suggesting this method is a generally-used method. Besides, we finish used H_2O_2 generated in this water oxidation system to reduce Cr(VI) in wastewater without by-products in a very short time and eco-friendly. 16.46 ppm of Cr(VI) could be reduced in 2 mins by using the generated H_2O_2 by H_2O_2 produced in the anode cell of system using CFP-$CuWO_4$&WO_3-Sb. Considering this method can generate H_2O_2 in oxygen-deficiency environment, it is a promosing strategy to be used a many different oxygen-deficiency situation, such as plateau and sewer and so on.

CRediT authorship contribution statement

Quan Zhou: Methodology, Formal analysis, experiment. **Zaoxue Yan:** Investigation, Resources, Data curation, Writing. **YangChun Lan:** Methodology, Resources. **Zheshun Ou:** Methodology, Formal analysis, Theoretical calculation. **Ruiting Hu:** Methodology, Data curation, experiment, Writing. **Xiaoli Wang** : Methodology, Formal analysis. **Zexi Yang** : Methodology, Formal analysis. **Yilin Chen:** Methodology, Formal analysis. **JunJie Cai:** Data Curation, Writing – review & editing. **Lejing Li:** Writing – review & editing,. **Qihong Lu:** Data curation, Writing – review & editing. **Shanquan Wang:** Data curation, Writing – review & editing. **Jimmy C. Yu:** Conceptualization. **Zhuofeng Hu:** Conceptualization, Writing – review & editing, Supervision, Funding acquisition, Theoretical calculation.

Declaration of Competing Interest

The authors declare that they have no known competing financial interests or personal relationships that could have appeared to influence the work reported in this paper.

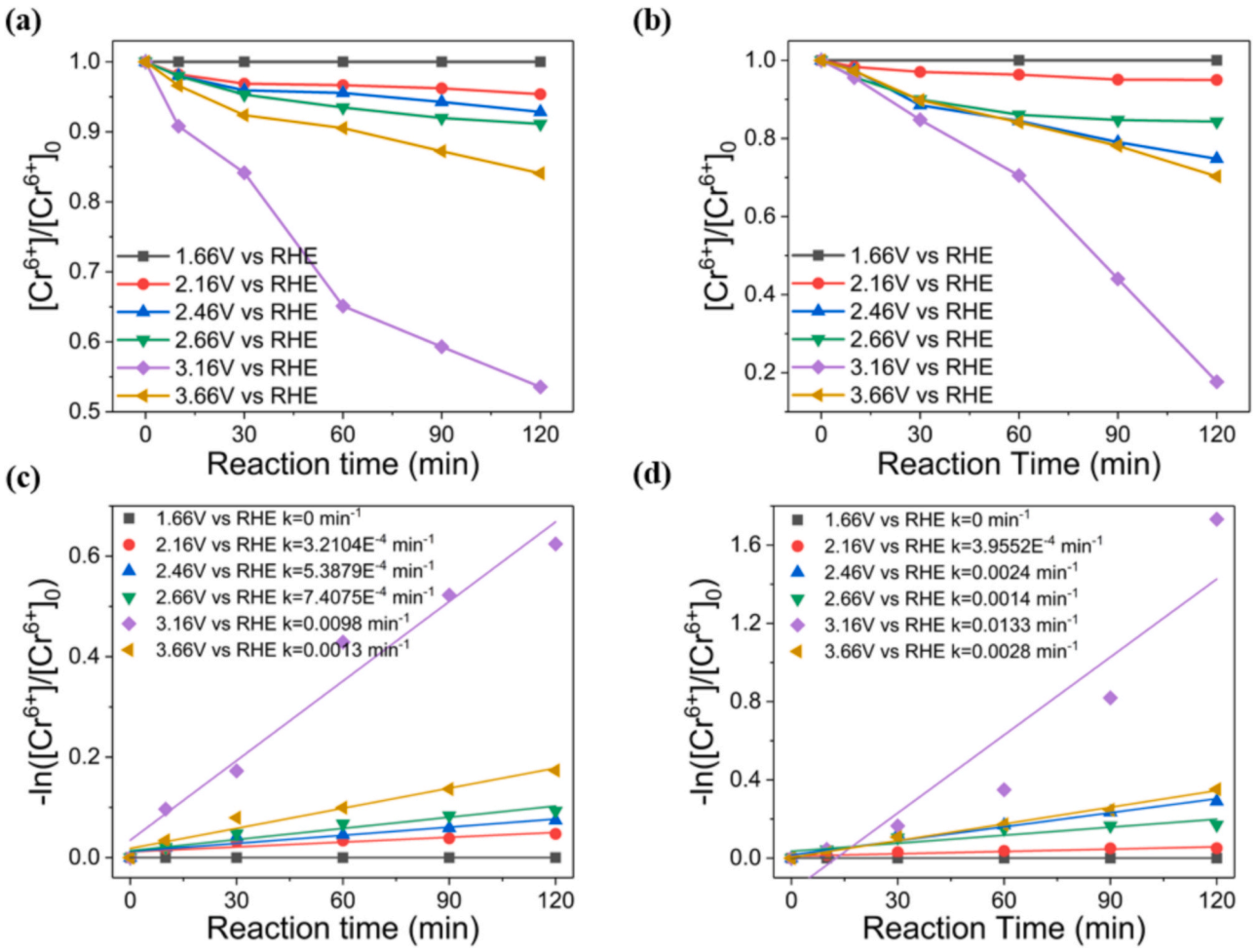

Fig. 10. Time profiles of 20 ppm of Cr(VI) reduction at different bias using (a, c) CFP-$CuWO_4$&WO_3 anode, (b, d) CFP-$CuWO_4$&WO_3-Sb anode.

Data availability

The data that has been used is confidential.

Acknowledgments

This work is supported by the Guangzhou Basic and Applied Basic Research Foundation, China (202201011695); the National Natural Science Foundation of China, China (Grant No. 51902357); the Natural Science Foundation of Guangdong Province, China (2019A1515012143); the Fundamental Research Funds for the Central Universities, Sun Yat-sen University, China (22lgqb23). We thank Dr. Xiongfei Huang for characterization equipment assistance. The theoretical calculation is supported by National supercomputer center in Guangzhou and National supercomputing center in Shenzhen (Shenzhen cloud computing center).

Appendix A. Supporting information

Supplementary data associated with this article can be found in the online version at doi:10.1016/j.apcatb.2023.123427.

References

[1] C.Y. Chen, X.L. Wang, B.J. Pan, W.Q. Xie, Q. Zhu, Y.L. Meng, Z.F. Hu, Q.M. Sun, Construction of a novel cascade electrolysis-heterocatalysis system by using zeolite-encaged ultrasmall palladium catalysts for H2O2 generation, Small 19 (2023), https://doi.org/10.1002/smll.202300114.

[2] Z. Yan, Y. Zhang, Z. Jiang, D. Jiang, W. Wei, Z. Hu, Nitrogen-doped bimetallic carbide-graphite composite as highly active and extremely stable electrocatalyst for oxygen reduction reaction in alkaline media, Adv. Funct. Mater. (2022), 2204031, https://doi.org/10.1002/adfm.202204031.

[3] L. Li, Z. Hu, Y. Kang, S. Cao, L. Xu, L. Yu, L. Zhang, J.C. Yu, Electrochemical generation of hydrogen peroxide from a zinc gallium oxide anode with dual active sites, Nat. Commun. 14 (2023), 1890, https://doi.org/10.1038/s41467-023-37007-9.

[4] L. Li, L. Xu, A.W.M. Chan, Z. Hu, Y. Wang, J.C. Yu, Direct hydrogen peroxide synthesis on a Sn-doped CuWO4/Sn anode and an air-breathing cathode, Chem. Mater. 34 (2022) 63–71, https://doi.org/10.1021/acs.chemmater.1c02787.

[5] L. Li, K. Xiao, P.K. Wong, Z. Hu, J.C. Yu, Hydrogen peroxide production from water oxidation on a CuWO4 anode in oxygen-deficient conditions for water decontamination, Acs Appl. Mater. Interfaces 14 (2022) 7878–7887, https://doi.org/10.1021/acsami.1c20834.

[6] L. Li, Z. Hu, J.C. Yu, On-demand synthesis of H(2)O(2)by water oxidation for sustainable resource production and organic pollutant degradation, Angew. Chem. -Int. Ed. 59 (2020) 20538–20544, https://doi.org/10.1002/anie.202008031.

[7] S. Kelly, X. Shi, S. Back, L. Vallez, S.Y. Park, S. Siahrostami, X. Zheng, J.K. Norskov, ZnO as an active and selective catalyst for electrochemical water oxidation to hydrogen peroxide, ACS Catal. 9 (2019) 4593–4599, https://doi.org/10.1021/acscatal.8b04873.

[8] T. Kang, B. Li, Q. Hao, W. Gao, F. Bin, K.N. Hui, D. Fu, B. Dou, Efficient hydrogen peroxide (H_2O_2) synthesis by CaSnO3 via two-electron water oxidation reaction, ACS Sustain. Chem. Eng. 8 (2020) 15005–15012, https://doi.org/10.1021/acssuschemeng.0c05449.

[9] S. Mavrikis, M. Göltz, S. Rosiwal, L. Wang, C. Ponce de León, Boron-doped diamond electrocatalyst for enhanced anodic H2O2 production, ACS Appl. Energy Mater. 3 (2020) 3169–3173, https://doi.org/10.1021/acsaem.0c00093.

[10] X. Shi, S. Back, T.M. Gill, S. Siahrostami, X. Zheng, Electrochemical synthesis of H2O2 by two-electron water oxidation reaction, Chem 7 (2021) 38–63, https://doi.org/10.1016/j.chempr.2020.09.013.

[11] X. Hu, Z. Sun, G. Mei, X. Zhao, B.Y. Xia, B. You, Engineering nonprecious metal oxides electrocatalysts for two-electron water oxidation to H2O2, Adv. Energy Mater. 12 (2022), 2201466, https://doi.org/10.1002/aenm.202201466.

[12] J. Baek, Q. Jin, N.S. Johnson, Y. Jiang, R. Ning, A. Mehta, S. Siahrostami, X. L. Zheng, Discovery of $LaAlO_3$ as an efficient catalyst for two-electron water

electrolysis towards hydrogen peroxide, Nat. Commun. 13 (2022), https://doi.org/10.1038/s41467-022-34884-4.
[13] X.J. Shi, S. Siahrostami, G.L. Li, Y.R. Zhang, P. Chakthranont, F. Studt, T. F. Jaramillo, X.L. Zheng, J.K. Norskov, Understanding activity trends in electrochemical water oxidation to form hydrogen peroxide, Nat. Commun. 8 (2017), 701, https://doi.org/10.1038/s41467-017-00585-6.
[14] L. Kihlborg, E. Gebert, CuWO4, a distorted Woiframite-type structure, Acta Cryst. B 26 (1970) 1020–1025.
[15] R. Diehl, G. Brandt, E. Salje, The crystal structure of triclinic WO_3, Acta Crystallogr. Sect. B Struct. Crystallogr. Cryst. Chem. 34 (1978) 1105–1111, https://doi.org/10.1107/s0567740878005014.
[16] A. Kuzmin, A. Kalinko, R.A. Evarestov, Ab initio LCAO study of the atomic, electronic and magnetic structures and the lattice dynamics of triclinic CuWO4, Acta Mater. 61 (2013) 371–378, https://doi.org/10.1016/j.actamat.2012.10.002.
[17] J.E. Yourey, B.M. Bartlett, Electrochemical deposition and photoelectrochemistry of $CuWO_4$, a promising photoanode for water oxidation, J. Mater. Chem. 21 (2011) 7651–7660, https://doi.org/10.1039/c1jm11259g.
[18] S.K. Pilli, T.G. Deutsch, T.E. Furtak, L.D. Brown, J.A. Turner, A.M. Herring, $BiVO_4$/$CuWO_4$ heterojunction photoanodes for efficient solar driven water oxidation, Phys. Chem. Chem. Phys. 15 (2013) 3273–3278, https://doi.org/10.1039/c2cp44577h.
[19] J. Rossmeisl, Z.W. Qu, H. Zhu, G.J. Kroes, J.K. Nørskov, Electrolysis of water on oxide surfaces, J. Electroanal. Chem. 607 (2007) 83–89, https://doi.org/10.1016/j.jelechem.2006.11.008.
[20] M.S. Burke, L.J. Enman, A.S. Batchellor, S. Zou, S.W. Boettcher, Oxygen evolution reaction electrocatalysis on transition metal oxides and (oxy)hydroxides: activity trends and design principles, Chem. Mater. 27 (2015) 7549–7558, https://doi.org/10.1021/acs.chemmater.5b03148.
[21] I.C. Man, H.Y. Su, F. Calle-Vallejo, H.A. Hansen, J.I. Martínez, N.G. Inoglu, J. Kitchin, T.F. Jaramillo, J.K. Nørskov, J. Rossmeisl, Universality in oxygen evolution electrocatalysis on oxide surfaces, ChemCatChem 3 (2011) 1159–1165, https://doi.org/10.1002/cctc.201000397.
[22] W.T. Hong, M. Risch, K.A. Stoerzinger, A. Grimaud, J. Suntivich, Y. Shao-Horn, Toward the rational design of non-precious transition metal oxides for oxygen electrocatalysis, Energy Environ. Sci. 8 (2015) 1404–1427, 10.1039/c4ee03869j.
[23] Z. Teng, Q. Zhang, H. Yang, K. Kato, W. Yang, Y.-R. Lu, S. Liu, C. Wang, A. Yamakata, C. Su, B. Liu, T. Ohno, Atomically dispersed antimony on carbon nitride for the artificial photosynthesis of hydrogen peroxide, Nat. Catal. 4 (2021) 374–384, https://doi.org/10.1038/s41929-021-00605-1.
[24] N. Fujiwara, T. Nagai, T. Ioroi, H. Arai, Z. Ogumi, Bifunctional electrocatalysts of lanthanum-based perovskite oxide with Sb-doped SnO2 for oxygen reduction and evolution reactions, J. Power Sources 451 (2020), https://doi.org/10.1016/j.jpowsour.2020.227736.
[25] Y. Wang, X. Lian, Y. Zhou, W. Guo, H. He, Synthesis and characterization of Sb2O3: a stable electrocatalyst for efficient H_2O_2 production and accumulation and effective degradation of dyes, N. J. Chem. 45 (2021) 8958–8964, https://doi.org/10.1039/D1NJ00637A.
[26] N. Zheng, X. He, R. Hu, W. Guo, Z. Hu, Co-activation of persulfate by cation and anion from FeP for advanced oxidation processes, Appl. Catal. B: Environ. 298 (2021), 120505, https://doi.org/10.1016/j.apcatb.2021.120505.
[27] L. Li, L. Xu, Z. Hu, J.C. Yu, Enhanced mass transfer of oxygen through a gas–liquid–solid interface for photocatalytic hydrogen peroxide production, Adv. Funct. Mater. 31 (2021), 2106120, https://doi.org/10.1002/adfm.202106120.
[28] L. Li, Z. Hu, J.C. Yu, On-demand synthesis of H2O2 by water oxidation for sustainable resource production and organic pollutant degradation, Angew. Chem. Int. Ed. 59 (2020) 20538–20544, https://doi.org/10.1002/anie.202008031.
[29] L. Xu, Y. Liu, L. Li, Z. Hu, J.C. Yu, Fabrication of a photocatalyst with biomass waste for H2O2 synthesis, Acs Catal. 11 (2021) 14480–14488, https://doi.org/10.1021/acscatal.1c03690.
[30] N.C. Zheng, X.H. Tang, Y.K. Lian, Z.S. Ou, Q. Zhou, R.L. Wang, Z.F. Hu, Low-valent copper on molybdenum triggers molecular oxygen activation to selectively generate singlet oxygen for advanced oxidation processes, J. Hazard. Mater. 452 (2023), https://doi.org/10.1016/j.jhazmat.2023.131210.
[31] U.E. Bollmann, A. Möller, Z. Xie, R. Ebinghaus, J.W. Einax, Occurrence and fate of organophosphorus flame retardants and plasticizers in coastal and marine surface waters, Water Res. 46 (2012) 531–538, https://doi.org/10.1016/j.watres.2011.11.028.
[32] P. Mäkie, P. Persson, L. Österlund, Solar light degradation of trimethyl phosphate and triethyl phosphate on dry and water-precovered hematite and goethite nanoparticles, J. Phys. Chem. C. 116 (2012) 14917–14929, https://doi.org/10.1021/jp3026732.
[33] E.A. Kozlova, P.G. Smirniotis, A.V. Vorontsov, Comparative study on photocatalytic oxidation of four organophosphorus simulants of chemical warfare agents in aqueous suspension of titanium dioxide, J. Photochem. Photobiol. a-Chem. 162 (2004) 503–511, https://doi.org/10.1016/s1010-6030(03)00392-7.
[34] Y. Aimer, O. Benali, K.G. Serrano, Study of the degradation of an organophosphorus pesticide using electrogenerated hydroxyl radicals or heat-activated persulfate, Sep. Purif. Technol. 208 (2019) 27–33, https://doi.org/10.1016/j.seppur.2018.05.066.